Progress In Electromagnetics Research B, Vol. 22, 359–377, 2010

NUMERICAL ANALYSIS OF HUMAN HEAD INTERACTION WITH PIFA ANTENNAS IN CELLULAR MOBILE COMMUNICATIONS

H. Khodabakhshi and A. Cheldavi

College of Electrical Engineering
Iran University of Science and Technology
Tehran, Iran

Abstract—This paper presents a numerical simulation of the human head coupling with a Planar Inverted-F Antenna (PIFA) structure based on the Coupled Integral Equation/Method of Moment (CIE/MoM) approach to study the effects of the EM coupling on the antenna performance. A mix-potential integral equation (MPIE) for the surface current of PIFA structure and a volume electric field integral equation (VEFIE) for the head with mutual coupling terms are obtained. Finally numerical results will be presented at 900 and 1800 MHz for the antenna performance parameters. The validity of the proposed method is evaluated using the XFDTD software.

1. INTRODUCTION

The ever increasing use of mobile phone in the vicinity of the human head has caused public concern about the potential health hazards due to electromagnetic (EM) radiation Besides, since the antenna is in close proximity to the human head, the strong EM coupling between the antenna and the nearby head will affect the performance of the handset antenna by changing the input impedance, the current distribution, the radiation pattern and the radiation efficiency of the antenna. So, the comprehensive understanding of the EM interaction between antenna and human head is necessary to improve antenna designs which are less susceptible to the human head tissue.

The interaction between handset antenna and human head can be studied using the sophisticated numerical methods, e.g., the Finite-Difference Time-Domain (FDTD) [1–7] the Method of Moment

Corresponding author: H. Khodabakhshi (khodabakhshi.hamid@gmail.com).

(MoM) [8], and the Eigen-function Expansion Method (EEM) [6]. Among these methods, the FDTD method has been widely used because of its ability of handling complex geometry of antennas and the nearby human tissues. In this method, an anatomical human head is usually used based on the magnetic resonance image (MRI) and important design parameters such as the antenna radiation patterns, input impedance, specific absorption rate (SAR) distribution have been with various antenna configurations. However, the FDTD suffers difficulties due to large storage and computation time if one desires to perform detailed parametric studies. Coupled integral equations (CIE) and the MoM have been employed to numerically solve the EM coupling between a realistically shaped 3-D man model and a proximate linear dipole [8]. The EEM methodology is based on the exact scattering solution of infinitesimal dipoles in the presence of a multi-layered lossy dielectric sphere and can be used for the parametric studies. The linear antennas such as half-wave dipole antenna are modeled as an array of small dipoles with unknown currents. Also, the EEM has been also combined with the MoM to take into account of the effects of the sphere on the current distribution along the antenna [9].

Extensive research results have been reported on the detailed EM coupling effects between dipole antenna and a human head model [6, 7]. Most previous works using the MoM for the antenna-head coupling problem have employed the simplified models of the head irradiated by the linear or helix antennas [8, 9] Also, in [11] the CIE/MoM approach has been used to study the detailed EM-coupling effects of a human-body model on the superquadric loop antennas at radio-paging bands. However, the EM coupling effects of a human head model using the MoM on more complex antenna such as Planar Inverted-F Antenna (PIFA) structures have not been reported.

In this paper, a numerical simulation scheme of the human head coupling with a PIFA structure is presented based on the CIE/MoM approach to study the effects of the EM coupling and head absorption on the antenna characteristics. In the CIE/MoM methodology, a mix-potential integral equation (MPIE) for the surface current of PIFA structure and a volume electric field integral equation (VEFIE) for the head with mutual coupling terms are obtained to model this EM-coupling problem. A homogenous spherical head model in the vicinity of the PIFA is used in the numerical simulation (Fig. 1) To apply the MoM to the CIE, we consider Roa-WiltonGlisson (RWG) [12] for the surface current of the PIFA as the basis functions and the induced electric field in the head is expanded as the pulse functions. Finally numerical results will be presented at 900 and 1800 MHz bands for the antenna performance parameters. Also, the situations of the PIFA with

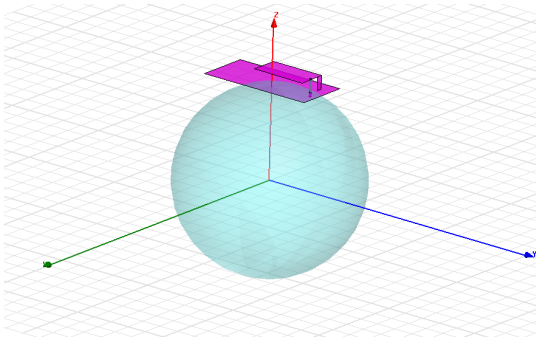

Figure 1. PIFA structure in the vicinity of a homogenous spherical head model.

different distances from the head in free-space and the vicinity of head model are studied and compared. The validity and accuracy of the proposed method is evaluated using the full-wave XFDTD software.

2. DERIVATION OF INTEGRAL EQUATIONS

Consider a lossy spherical head model with electrical parameters $(\sigma(\vec{r}), \varepsilon(\vec{r}), \mu_0)$ exposed to the near field of a PIFA as shown in Fig. 1. A PIFA is a post loaded rectangular microstrip antenna fed by a prob. This antenna has been suggested for mobile telephone handsets because of its compactness and low profile [13]. The size of PIFA with the post located at a corner of a rectangular plate can be determined approximately from [13]

$$f_r = \frac{c}{4\,(L+W)} \tag{1}$$

where c is the speed of light, L and W are the dimensions of the element, and f_r is the operating frequency.

The probe feed of the PIFA creates the surface current density $\mathbf{J}_s(\vec{r}\,')$ on the PIFA and therefore the electric field $\mathbf{E}^a$ radiated from the antenna induces an equivalent free-space current density $\mathbf{J}_{eq}$ inside the sphere. The equivalent current density inside the lossy sphere gives rise to a scattered field $\mathbf{E}^s$ and is given by

$$\mathbf{J}_{eq}\,(\vec{r}\,) = [\sigma\,(\vec{r}\,) + j\omega\,(\varepsilon\,(\vec{r}\,) - \varepsilon_0)]\,\mathbf{E}\,(\vec{r}\,) = \tau\,(\vec{r}\,)\,\mathbf{E}\,(\vec{r}\,), \tag{2}$$

where $\mathbf{E}(\vec{r})$ is the total electric field inside the head and equals to the sum of the incident field radiated $\mathbf{E}^a$ by the PIFA and the scattered field $\mathbf{E}^s$ from the spherical head and is given by

$$\mathbf{E}\,(\vec{r}\,) = \mathbf{E}^s\,(\vec{r}\,) + \mathbf{E}^a\,(\vec{r}\,) \tag{3}$$

Using the dyadic Green's function approach, the scattered electric field $\mathbf{E}^s$ inside the volume V of the sphere can be written as [14]

$$\mathbf{E}^s(\vec{r}) = P.V \int_V \mathbf{J_{eq}}(\vec{r}') \cdot \bar{\bar{\mathbf{G}}}_o(\vec{r}, \vec{r}')\, dv' - \frac{\mathbf{J_{eq}}}{j3\omega\varepsilon_0} \tag{4}$$

where $P.V$ represents the principal value of the integral.

Substituting (2) and (4) in (3), one gets

$$\left[1 + \frac{\tau(\vec{r})}{3j\omega\varepsilon_0}\right]\mathbf{E}(\vec{r}) - P.V \int_V \tau(\vec{r}')\,\mathbf{E}(\vec{r}') \cdot \bar{\bar{\mathbf{G}}}_o(\vec{r}, \vec{r}')\, dv' = \mathbf{E}^a(\vec{r}) \tag{5}$$

where $\bar{\bar{\mathbf{G}}}_o(\vec{r}, \vec{r}')$ is given by [14]

$$\begin{aligned} \bar{\bar{\mathbf{G}}}_o(\vec{r}, \vec{r}') &= -j\omega\mu_0 \left[\bar{\bar{\mathbf{I}}} + \frac{\nabla\nabla}{k_0^2}\right] \psi(\vec{r}, \vec{r}'), \\ \psi(\vec{r}, \vec{r}') &= \frac{\exp(-jk_0 |\vec{r} - \vec{r}'|)}{4\pi |\vec{r} - \vec{r}'|}. \end{aligned} \tag{6}$$

The electric field $\mathbf{E}^a$ radiated from the antenna can be obtained as

$$\mathbf{E}^a = -j\omega\mathbf{A} - \nabla\varphi \tag{7}$$

where $\mathbf{A}$ and φ are the magnetic vector potential and the scalar potential, respectively and are obtained as

$$\begin{aligned} \mathbf{A}(\vec{r}) &= \mu_0 \int_{S_a} \mathbf{J}_s(\vec{r}')\psi(\vec{r}, \vec{r}')\, ds' \\ \varphi(\vec{r}) &= \frac{1}{\varepsilon_0} \int_{S_a} \rho_s(\vec{r}')\psi(\vec{r}, \vec{r}')\, ds' = \frac{-1}{j\omega\varepsilon_0} \int_{S_a} \nabla' \cdot \mathbf{J}_s(\vec{r}')\psi(\vec{r}, \vec{r}')\, ds'. \end{aligned} \tag{8}$$

Combining (6)–(8) and (5) gives the following tensor integral equation for $\mathbf{E}(\vec{r})$ and $\mathbf{J}_s(\vec{r})$

$$\begin{aligned} &-j\omega\mu_0 \int_{S_a} \mathbf{J}_s(\vec{r}')\psi(\vec{r}, \vec{r}')\, ds' + \frac{1}{j\omega\varepsilon_0} \nabla \int_{S_a} \nabla' \cdot \mathbf{J}_s(\vec{r}')\psi(\vec{r}, \vec{r}')\, ds' \\ &+ P.V \int_V \tau(\vec{r}')\,\mathbf{E}(\vec{r}') \cdot \bar{\bar{\mathbf{G}}}_o(\vec{r}, \vec{r}')\, dv' - \left[1 + \frac{\tau(\vec{r})}{3j\omega\varepsilon_0}\right]\mathbf{E}(\vec{r}) = 0, \end{aligned} \tag{9}$$

The tensor integral Equation (9) contains three scalar integral equations.

The boundary condition for the electric field on the surface of the PIFA requires

$$\hat{n} \times \left(\mathbf{E}^i(\mathbf{J}_i) + \mathbf{E}^a + \mathbf{E}^s\right)|_{on\ Antenna=0} \tag{10}$$

Since the field point $\vec{r}$ in (4) is not inside the volume V of the sphere (source region), the principal value ($P.V$) and the correction term $-\mathbf{J_{eq}}/j3\omega\varepsilon_0$ are not required. So, (10) can be written as

$$\hat{n}\times\left(-j\omega\mu_{\mathbf{0}}\int\limits_{S}\mathbf{J}_s\left(\vec{r}\,'\right)\psi(\vec{r},\vec{r}\,')ds'+\frac{1}{j\omega\varepsilon_0}\nabla\int\limits_{S}\nabla'\cdot\mathbf{J}_s\left(\vec{r}\,'\right)\psi\left(\vec{r},\vec{r}\,'\right)ds'\right.$$
$$\left.+\int\limits_{V_b}\tau\left(\vec{r}\,'\right)\mathbf{E}\left(\vec{r}\,'\right)\cdot\bar{\bar{\mathbf{G}}}_o\left(\vec{r},\vec{r}\,'\right)dv'\right)_{on\ Antenna}=-\hat{n}\times\mathbf{E}^i. \tag{11}$$

where $\mathbf{E}^i$ is the impressed field from the probe feed.

The total electric field $\mathbf{E}$ inside the head and the surface current density $\mathbf{J}_s(\vec{r}\,')$ on the PIFA in the coupled integral Equations (9) and (11) are unknown quantities and are to be determined by MoM in Section 3.

3. MOMENT-METHOD SOLUTION

Equations (9) and (11) are two complicated coupled integral equations but they can be solved numerically using MoM. The surface of the PIFA is divided into N_a separate triangles. Each pair of triangles has a common edge that constitutes the corresponding RWG edge element [12] as shown in Fig. 2. One of the triangles has a plus sign and the other a minus sign. A vector function is assigned to the nth edge element [12, 15]:

$$\mathbf{f}_n\left(\vec{r}\right)=\begin{cases}\dfrac{l_n}{2A_n^+}\boldsymbol{\rho}_n^+\left(\vec{r}\right) & \vec{r}\in T_n^+\\ \dfrac{l_n}{2A_n^-}\boldsymbol{\rho}_n^-\left(\vec{r}\right) & \vec{r}\in T_n^-\\ 0 & \text{otherwise}\end{cases} \tag{12}$$

where l_n is the nth edge length and $A_n^{\pm}$ is the area of triangle $T_n^{\pm}$. Vectors $\boldsymbol{\rho}_n^{\pm}$ are shown in Fig. 2(b). Vector $\boldsymbol{\rho}_n^+$ connects the free vertex of the plus triangle to the observation point $\vec{r}$ and the vector $\boldsymbol{\rho}_n^-$ connects the observation point to the free vertex of the minus triangle.

The unknown surface current of the PIFA is a sum of the basis function (12) over all edge elements with unknown coefficients I_n as follow

$$\mathbf{J}_s\left(\vec{r}\right)=\sum_{n=1}^{N_a}I_n\mathbf{f}_n\left(\vec{r}\right) \tag{13}$$

The head is partitioned into a finite number N of cubic cells inside each of which $\mathbf{E}(\vec{r})$ is regarded as constant. The induced electric field in the head is expanded in terms of the pulse functions

$$\mathbf{E}(\vec{r}) = \hat{x}\sum_{n=1}^{N} E_x^n p_n(\vec{r}) + \hat{y}\sum_{n=1}^{N} E_y^n p_n(\vec{r}) + \hat{z}\sum_{n=1}^{N} E_z^n p_n(\vec{r}) \tag{14}$$

where I_n, E_x^n, E_y^n, E_z^n in (13) and (14) are unknown coefficients to be determined.

Substituting (12), (13) and (14) in integral Equation (9), one gets

$$\begin{aligned}
&-j\omega\mu_0 \sum_{n=1}^{N_a} I_n \left(\frac{l_n}{2A_n^+} \int_{T_n^+} \boldsymbol{\rho}_n^+(\vec{r}\,')\psi(\vec{r},\vec{r}\,')\,ds' + \frac{l_n}{2A_n^-} \int_{T_n^-} \boldsymbol{\rho}_n^-(\vec{r}\,')\psi(\vec{r},\vec{r}\,')\,ds' \right) \\
&+ \frac{1}{j\omega\varepsilon_0} \sum_{n=1}^{N_a} I_n \left(\frac{l_n}{A_n^+} \int_{T_n^+} \nabla\psi(\vec{r},\vec{r}\,')ds' - \frac{l_n}{A_n^-} \int_{T_n^-} \nabla\psi(\vec{r},\vec{r}\,')ds' \right) \\
&+ \sum_{p=1}^{3} \hat{x}_p \left\{ \sum_{n=1}^{N} \left[\sum_{q=1}^{3} E_{x_q}^n \tau_n PV \int_{V_n} G_{x_p x_q}(\vec{r},\vec{r}\,')\,dv' \right.\right. \\
&\left.\left. - \left(1 + \frac{\tau(\vec{r})}{3j\omega\varepsilon_0}\right) E_{x_p}^n p_n(\vec{r}) \right] \right\} = 0
\end{aligned} \tag{15}$$

where $x_1 = x$, $x_2 = y$, $x_3 = z$.

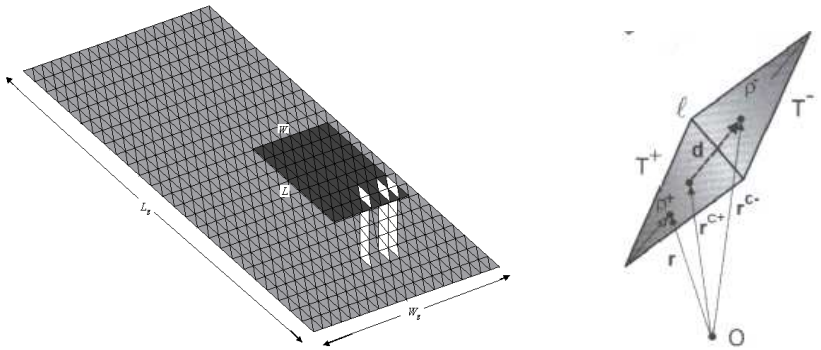

(a) (b)

Figure 2. (a) PIFA structure with triangular meshes. (b) RWG edge element.

By applying the point-matching technique to (15) at the center of each head cell, and after some manipulation we have

$$\sum_{n=1}^{N_a} I_n(-j\omega\mathbf{B}_{mn}+\mathbf{\Psi}_{mn})+\sum_{p=1}^{3}\hat{x}_p\sum_{n=1}^{N}\sum_{q=1}^{3}E_{x_q}^{n}G_{x_px_q}^{mn}=0 \;\; m=1,2,\ldots,N, \quad (16)$$

where

$$\begin{aligned}
\mathbf{B}_{mn} &= \frac{\mu_0}{4\pi}\left[\frac{l_n}{2A_n^+}\int\limits_{T_n^+}\boldsymbol{\rho}_n^+\left(\vec{r}\,'\right)\psi_m\left(\vec{r}\,'\right)ds'+\frac{l_n}{2A_n^-}\int\limits_{T_n^-}\boldsymbol{\rho}_n^-\left(\vec{r}\,'\right)\psi_m\left(\vec{r}\,'\right)ds'\right]\\
\mathbf{\Psi}_{mn} &= \frac{1}{4\pi j\omega\varepsilon_0}\left(\frac{l_n}{A_n^+}\int\limits_{T_n^+}\mathbf{g}_m\left(\vec{r}\,'\right)ds'-\frac{l_n}{A_n^-}\int\limits_{T_n^-}\mathbf{g}_m(\vec{r}\,')ds'\right)\\
G_{x_px_q}^{mn} &= \tau_n PV\cdot\int\limits_{V_n}G_{x_px_q}\left(\vec{r}_m,\vec{r}\,'\right)dv'-\delta_{pq}\delta_{mn}\left(1+\frac{\tau(\vec{r})}{3j\omega\varepsilon_0}\right)\\
\psi_m\left(\vec{r}\,'\right) &= \frac{\exp\left(-jk_0R_m\right)}{R_m}\\
\mathbf{g}_m\left(\vec{r}\,'\right) &= \psi_m(\vec{r}\,')\cdot\left(\frac{-jk_0}{R_m}-\frac{1}{R_m^2}\right)\left(\vec{r}_m-\vec{r}\,'\right)\\
R_m &= \left|\vec{r}_m-\vec{r}\,'\right|.
\end{aligned} \quad (17)$$

Substituting (12), (13) and (14) in integral Equation (11), it leads

$$\begin{aligned}
&\hat{n}\times\left[-j\omega\mu_0\sum_{n=1}^{N_a}I_n\left(\frac{l_n}{2A_n^+}\int\limits_{T_n^+}\boldsymbol{\rho}_n^+(\vec{r}\,')\psi(\vec{r},\vec{r}\,')ds'+\frac{l_n}{2A_n^-}\int\limits_{T_n^-}\boldsymbol{\rho}_n^-(\vec{r}\,')\psi(\vec{r},\vec{r}\,')ds'\right)\right.\\
&+\frac{1}{j\omega\varepsilon_0}\sum_{n=1}^{N_a}I_n\left(\frac{l_n}{A_n^+}\int\limits_{T_n^+}\nabla\psi(\vec{r},\vec{r}\,')ds'-\frac{l_n}{A_n^-}\int\limits_{T_n^-}\nabla\psi(\vec{r},\vec{r}\,')ds'\right)\\
&\left.+\sum_{n=1}^{N}\sum_{p=1}^{3}E_{x_p}^{n}\int\limits_{V_n}\tau_n\hat{x}_p\cdot\bar{\bar{\mathbf{G}}}_o\left(\vec{r},\vec{r}\,'\right)dv'\right]_{on\ Antenna}=-\hat{n}\times\mathbf{E}^i
\end{aligned} \quad (18)$$

where $x_1 = x$, $x_2 = y$, $x_3 = z$.

By taking the scalar products of (18) with the weighting functions $\mathbf{w}_m(\vec{r}) = \mathbf{f}_m(\vec{r})$, $m = 1, 2, \ldots, N_a$ (Galerkin technique) and after some

calculation, it leads to

$$l_m \sum_{n=1}^{N_a} I_n \left[j\omega \left(\mathbf{A}_{mn}^{+} \cdot \frac{\boldsymbol{\rho}_m^{c+}}{2} + \mathbf{A}_{mn}^{-} \cdot \frac{\boldsymbol{\rho}_m^{c-}}{2} \right) + \Phi_{mn}^{-} - \Phi_{mn}^{+} \right]$$
$$+ l_m \sum_{n=1}^{N} \sum_{p=1}^{3} E_{x_p}^{n} \left(\mathbf{G}_{mn}^{+} \cdot \frac{\boldsymbol{\rho}_m^{c+}}{2} + \mathbf{G}_{mn}^{-} \cdot \frac{\boldsymbol{\rho}_m^{c-}}{2} \right) = V_m, \quad m = 1, 2, ..., N_a \quad (19)$$

where

$$\mathbf{A}_{mn}^{\pm} = \frac{\mu_0}{4\pi} \left[\frac{l_n}{2A_n^{+}} \int\limits_{T_n^{+}} \boldsymbol{\rho}_n^{+}(\vec{r}\,') \psi_m^{\pm}(\vec{r}\,') ds' + \frac{l_n}{2A_n^{-}} \int\limits_{T_n^{-}} \boldsymbol{\rho}_n^{-}(\vec{r}\,') \psi_m^{\pm}(\vec{r}\,') ds' \right]$$

$$\Phi_{mn}^{\pm} = -\frac{1}{4\pi j\omega\varepsilon_0} \left(\frac{l_n}{A_n^{+}} \int\limits_{T_n^{+}} \psi_m^{\pm}(\vec{r}\,') ds' - \frac{l_n}{A_n^{-}} \int\limits_{T_n^{-}} \psi_m^{\pm}(\vec{r}\,') ds' \right) \quad (20)$$

$$\psi_m^{\pm}(\vec{r}\,') = \frac{\exp\left(-jk_0 \left| \vec{r}_m^{c\pm} - \vec{r}\,' \right| \right)}{\left| \vec{r}_m^{c\pm} - \vec{r}\,' \right|},$$

$$\mathbf{G}_{mn}^{\pm} = \sum_{q=1}^{3} \hat{x}_q \int\limits_{V_n} \tau_n G_{x_p x_q} \left(\vec{r}_m^{\,c\pm}, \vec{r}\,' \right) dv',$$
$$V_m = \int\limits_{T_m^{+}+T_m^{-}} \mathbf{E}^i \cdot \mathbf{f}_m ds = V_0 \int\limits_{T_m^{+}+T_m^{-}} \delta(z) \hat{n} \cdot \mathbf{f}_m ds = \begin{cases} l_n V_0 & m = n \\ 0 & \text{otherwise} \end{cases} \quad (21)$$

where $\boldsymbol{\rho}_m^{c\pm}$ are the vectors between the free vertex point and the centroid point $\vec{r}_m^{\,c\pm}$ of the two triangles $T_m^{\pm}$ of the edge element m, respectively.

The thin-strip model is used as the probe feed and this probe feed model can be easily adapted to RWG edge elements [15]. For a thin strip the radius of the equivalent cylindrical wire is $a_{eq} = 0.25s$, where s is the strip width [15]. A model of the strip-plate junction is shown in Fig. 3. There are two edge elements that have the common edge l_m The imposed voltage at the feeding edge l_m is V_0 (bottom-driven probe).

The $G_{x_p x_q}$ in (17) and (21) is the element of the matrix representation of the Dyadic Green's function $\bar{\bar{\mathbf{G}}}_o(\vec{r}, \vec{r}\,')$ in (5) and can

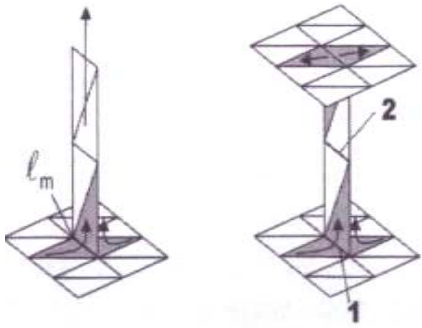

Figure 3. Model of the probe feed [15].

be obtained as [11]

$$\begin{aligned} &G_{x_p x_q} \\ &= \frac{-j\omega\mu_0 k_0}{4\pi\alpha^3} e^{-j\alpha}\left[\left(\alpha^2-1-j\alpha\right)\delta_{pq}+(x_p-x'_p)(x_q-x'_q)\left(3-\alpha^2+3j\alpha\right)/R^2\right] \\ &\alpha = k_0 R, \quad R = \left|\vec{r}-\vec{r}'\right| \quad \vec{r} = [x_1, x_2, x_3], \quad \vec{r}' = \left[x'_1, x'_2, x'_3\right]. \end{aligned} \tag{22}$$

Equations (16) and (19) can be converted into a matrix form. The volume integrals in (17) are computed by Gaussian quadrature integral method. Combining (16) and (19), we have $N_a + 3N$ simultaneous algebraic equations which can be expressed in a matrix form as follows:

$$\begin{pmatrix} \mathbf{Z_1} & \vdots & \mathbf{Z_2} \\ \cdots & \cdots & \cdots \\ \mathbf{Z_3} & \vdots & \mathbf{Z_4} \end{pmatrix} \begin{bmatrix} I_1 \\ I_2 \\ \vdots \\ I_{N_a} \\ \cdots \\ [E_x] \\ [E_y] \\ [E_z] \end{bmatrix} = \begin{bmatrix} 0 \\ 0 \\ \vdots \\ l_n V \\ 0 \\ \vdots \\ 0 \end{bmatrix} \tag{23}$$

In (23) the $(N_a + 3N) \times (N_a + 3N)$ matrix consists of four submatrices: $[Z_1]$ is a $N_a \times N_a$ matrix, $[Z_2]$ is a $N_a \times 3N$ matrix, $[Z_3]$ is a $3N \times N_a$ matrix and $[Z_4]$ is a $3N \times 3N$ matrix. The unknown surface current of the PIFA and the induced electric fields into the head are then determined by solving the above matrix equation.

After determination of the surface current of the PIFA, the input impedance of the antenna can be obtained as

$$Z_{in} = \frac{V_0}{I_{in}} \tag{24}$$

where V is the imposed voltage at feeding edge and I_{in} is the sum of the currents of two edge elements corresponding to l_m (Fig. 3).

The input power to the antenna P_i and the power absorbed P_{abs} by the head can be determined as

$$P_i = \frac{1}{2}\mathrm{Re}\left(V I_{in}^*\right), \quad P_{abs} = \int\limits_V \frac{1}{2}\sigma \left|\mathbf{E}\right|^2 dv. \tag{25}$$

The total radiation field (to free-space) is the sum of the field radiated by the PIFA and the scattered field from the spherical head. So, the radiated power to the far-field region P_{rad} and the directivity of an antenna are obtained as [13]

$$P_{rad} = \oint\limits_s \frac{1}{2}\mathrm{Re}\left[\mathbf{E}^r \times \mathbf{H}^{r^*}\right] \cdot \hat{n} ds, \quad D\left(\theta,\varphi\right) = \frac{4\pi r^2 p\left(\theta,\varphi\right)}{P_{rad}} \tag{26}$$

where $p(\theta,\varphi)$ is the radiated power density.

Since the input power to the antenna should be equal to the sum of the head absorbed power and the radiation power to free-space, so it can be used to check the EM coupling computation accuracy. The computation error is defined as [8]

$$\text{computation error} = \frac{\left|P_i - \left(P_{abs} + P_{rad}\right)\right|}{P_i}. \tag{27}$$

The radiation efficiency of the antenna-head system can be defined as

$$\eta_a = \frac{P_{rad}}{P_{abs} + P_{rad}}. \tag{28}$$

The total antenna efficiency η_t can be obtained as the product of the reflection efficiency $(1 - |\Gamma|^2)$, conduction efficiency, dielectric efficiency, and antenna-head efficiency. Also, the power gain of an antenna G_p can be written as $G_p = \eta_t \times D$.

4. NUMERICAL RESULTS AND DISCUSSION

In this section, we present two PIFA structures in the vicinity of a homogenous spherical head model at 900 and 1800 MHz. The PIFA is located at 5 mm away from the surface of the spherical head (Fig. 1). The radius of the sphere head model is assumed 9 cm. The electrical parameters of the homogenous spherical head model at 900 and 1800 MHz are shown in Table 1 [14].

The dimensions of the PIFA structures (Fig. 2(a)) at 900 and 1800 MHz can be determined using (1). The PIFA structures are designed with the following geometric parameters: $L = 6$ cm, $W =$

Table 1. The electrical parameters of the homogenous spherical head model from [17].

	ε_r	σ	density (kg/m^3)
900 MHz	41.5	0.97	1000
1800 MHz	40	1.4	1000

2.8 cm, $h = 1.3$ cm, $L_g = 11.6$ cm, $W_g = 5.2$ cm at 900 MHz and $L = 2.8$ cm, $W = 1.6$ cm, $h = 1.3$ cm, $L_g = 10$ cm, $W_g = 4$ cm at 1800 MHz. The width of the post plates of the PIFA is selected as 6 mm and 4 mm at 900 and 1800 MHz, respectively.

The surface of the PIFA structures is subdivided into N_a separate triangles. The number of the edge elements is chosen as 1409 and 1635 for PIFA900 and PIFA1800, respectively. A uniform cubic cell of edge length of 1.2 cm was used for modeling the human head (Fig. 4).

Table 2 gives the numerical results of the antenna radiation and the head absorption of a 900 MHz PIFA in free space and in the vicinity of the head. It is observed that, in all cases, the computation errors are lower than 2%. So, the sum of the radiated power and the absorbed power is almost equal to the antenna input power. Also, because of the power absorption in the head, about 71–92% of the antenna input power is radiated into free space for different antenna-head distances. A stronger EM coupling of the closer distance increases the head absorption power. Therefore, the less the antenna input power is radiated to free space in the closer distance to the head.

Figure 5 shows the return loss ($R.L$) and input impedance of PIFA in 900 MHz band (GSM900) for head-antenna separation of 5 mm. Due to the small antenna-head separation, strong EM coupling between the

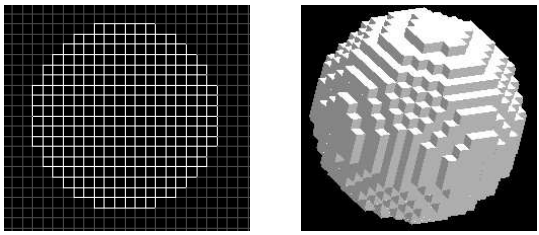

Figure 4. (a) A "cubic sphere" constructed from 1088 cubic cells, (b) side view of the "cubic sphere".

Table 2. Comparison of the PIFA radiation and head absorption power in free space and in the proximity of the head at 900 MHz.

PIFA 900 MHz	Free space		In the vicinity of the head model				
Separation distance (d)		5 mm	10 mm	20 mm	30 mm	40 mm	50 mm
Input Impedance (Z_{in})	72.6–j7.1	74.8+j4.6	78.2+j2.4	81.3–j1.9	81.8-j5.5	80.9–j8.2	79.6–j10.3
Radiation Power (W)	1	0.726	0.759	0.831	0.894	0.913	0.923
Absorbed Power (W)	----	0.293	0.232	0.158	0.120	0.099	0.086
Radiation Efficiency (%)	100	71.2	76.6	84.0	88.2	90.2	91.5
Computational Error (%)	0	1.94	0.833	1.03	1.42	1.18	0.92

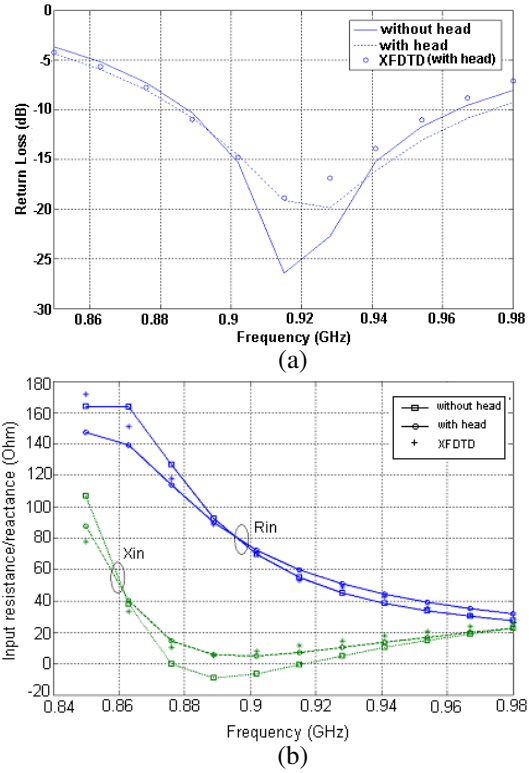

Figure 5. (a) Return loss of PIFA 900, (b) input resistance and reactance of PIFA 900.

PIFA and the nearby head affects the input impedance of the antenna. So, the input impedance shifts from the resonance. Since the loss is increased in the presence of the head, the Q of the antenna decreases and as a result, the bandwidth is slightly enhanced.

As shown in Fig. 5(a), the voltage standing wave ratio (VSWR) is less than 2.5 ($R.L < -7.36\,\text{dB}$) in GSM-900 with and without the spherical head. Also, a good agreement is observed between the results

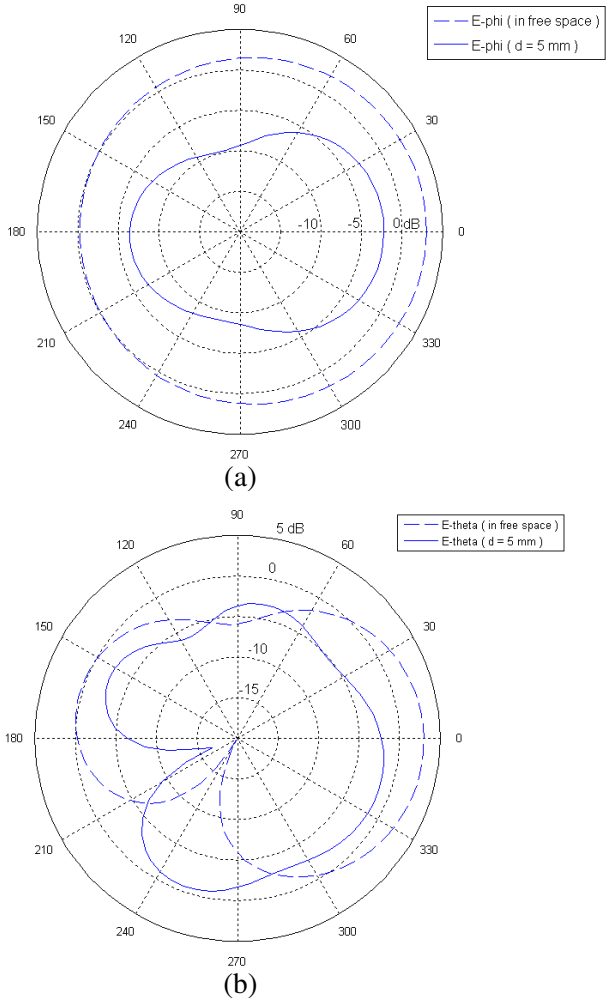

Figure 6. Radiation patterns of the PIFA at 900 MHz. (a) Horizontal plane (x-z plane), (b) vertical plane (y-z plane).

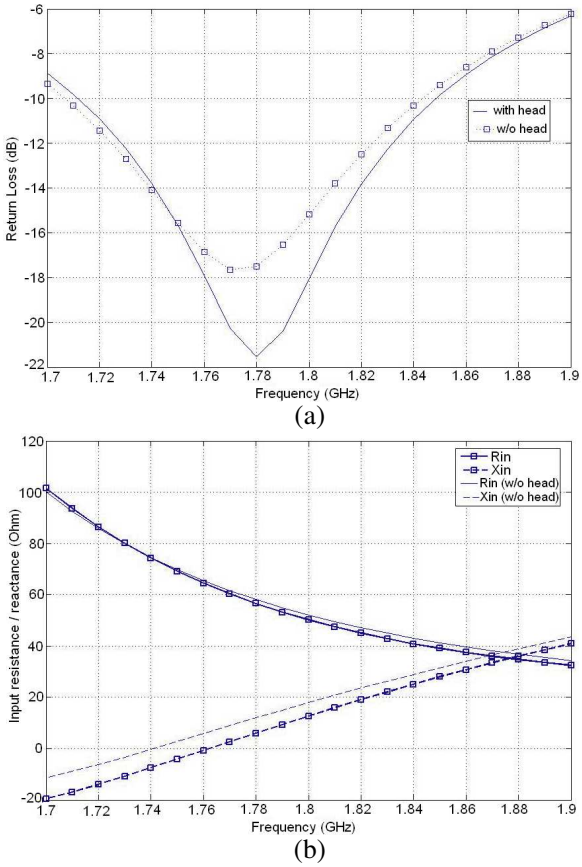

Figure 7. (a) Return loss of PIFA 1800, (b) input resistance and reactance of PIFA 1800.

of the proposed method and the results of the full-wave XFDTD [20] software. The execution time of the proposed method, using MATLAB software, on a desktop computer with 2 GHz Pentium-IV processor and 1 GB RAM is about 13 minutes while the running time of the XFDTD with the cell size of $1\,\text{mm} \times 1\,\text{mm} \times 1\,\text{mm}$ is approximately 2 hours and 42 minutes for each frequency It is obvious that this method is very efficient in terms of the running time and the computation load.

The radiation pattern of the PIFA with and without the head at 900 MHz is shown in Fig. 6. As can be seen in the figure, the gain patterns are significantly changed in the presence of the head. As expected, the spherical head model disturbs the symmetry of the radiation pattern in the horizontal plane. In the x-z plane, the peak

field intensity in the $\theta = 0$ direction decreases as 5 dB, and drops by 7 dB in the direction of the head. High attenuation of the radiation field toward the spherical head direction is observed. Also, it is seen that the antenna gain reduces as compared to the gain of antenna in free space. This should be considered in the antenna design and link budget of the cellular mobile communication.

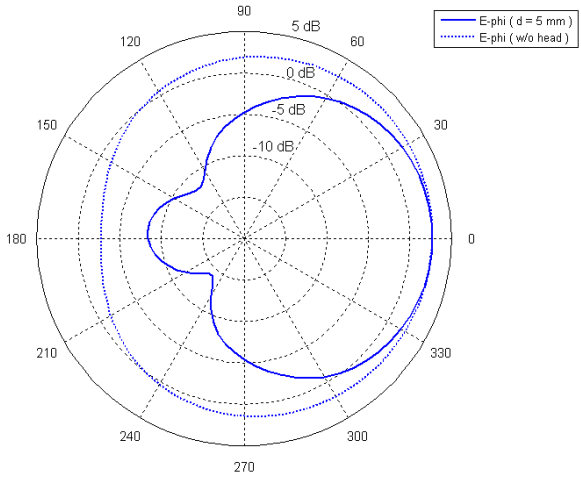

(a)

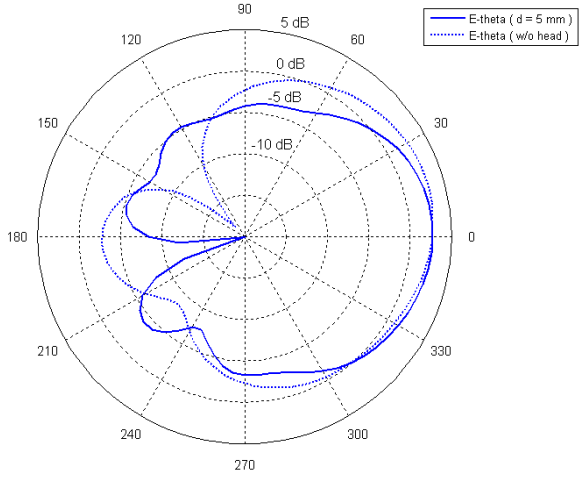

(b)

Figure 8. Radiation patterns of the PIFA at 1800 MHz. (a) Horizontal plane (x-z plane), (b) vertical plane (y-z plane).

The $R.L$ and input impedance of PIFA in GSM-1800 band for head-antenna separation of 5 mm is shown in Fig. 7. Similar to 900 MHz band, due to the small antenna-head separation, strong EM coupling between the PIFA and the nearby head affects the input impedance of the antenna. So, the input impedance shifts from the resonance. But the input impedance in GSM-1800 band varies more slowly than it in GSM-900 band. Also, the spherical head affects on the input impedance at 900 MHz band more than it at 1800 MHz band (especially input resistance). Since the loss is increased in the presence of the head, the Q of the antenna decreases and as a result, the bandwidth is slightly enhanced. As shown in Fig. 7(a), the VSWR is less than 2.5 ($R.L < -7.36$ dB) in GSM-1800 in both cases.

The radiation pattern of the PIFA with and without the head at 1800 MHz is shown in Fig. 8. It is seen that the gain patterns are significantly changed in the presence of the head, but the effect of the spherical head model on the radiation patterns at 1800 MHz is noticeably less than it at 900 MHz. Again, the spherical head model disturbs the symmetry of the radiation pattern in the horizontal plane. In the x-z plane, the peak field intensity in the direction of the head direction decreases as 6 dB, but it does not drop in the $\theta = 0$ direction. Also, it is seen that the antenna gain reduces as compared to the gain of antenna in free space, but the gain reduction at 1800 MHz is less than it at 900 MHz.

The input impedance of the PIFA at 900 and 1800 MHz is plotted as function of the head-antenna separation in Fig. 9. As shown in the figure the input impedance versus the antenna-head separation

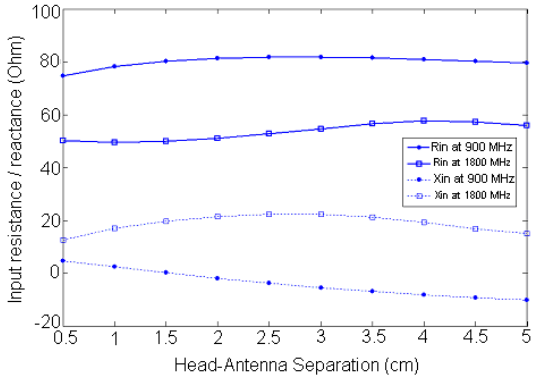

Figure 9. Input resistance/reactance of the PIFA at 900 and 1800 MHz versus antenna-head distance.

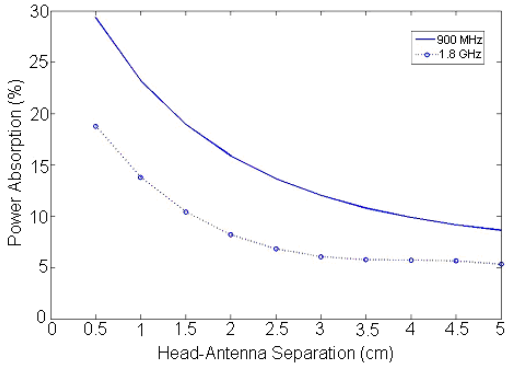

Figure 10. Power absorption in the homogenous spherical head as function of the head-antenna distance at 900 and 1800 MHz.

distance at 900 MHz varies more slowly than it at 1800 MHz. Also, the variation of the input reactance is more than the variation of the input resistance.

The power absorption in the homogenous spherical head at 900 and 1800 MHz versus the head-antenna distance is shown in Fig. 10. One can observe that the power absorption is strongly dependent on the head-antenna distance (d) and the absorbed power at 1800 MHz is lower than the power absorption at 900 MHz. When the antenna is located near the head, noticeable part of the delivered power to antenna is absorbed in the spherical head (29% at 900 MHz and 19% at 1800 MHz for $d = 5$ mm), but the absorbed power at larger distance becomes smaller (8% at 900 MHz and 5% at 1800 MHz for $d = 5$ cm).

5. CONCLUSION

In this paper, electromagnetic (EM) coupling between a PIFA structure and a homogenous spherical head model has been investigated at 900 and 1800 MHz bands. The CIE/MoM approach was used to study the effects of the EM coupling on the antenna characteristics. A mix-potential integral equation (MPIE) for the surface current of PIFA structure and a volume electric field integral equation (VEFIE) for the head with mutual coupling terms were obtained to model this EM-coupling problem. The RWG function was considered for the surface current of the PIFA as the basis functions and the induced electric field in the head was expanded as the pulse functions. Finally the numerical results have been presented at 900 and 1800 MHz for the antenna performance parameters. It was observed that the input

impedance of the antenna changes slightly in the presence of the head. Also, the radiation patterns deform significantly and the spherical head model disturbs the symmetry of the radiation pattern in the horizontal plane. The peak gain in the direction of the head decreases as much as 7 dB and 5 dB at 900 and 1800 MHz, respectively It was seen that the proposed method was very efficient in terms of the running time and the computation load. So it can be used for the parametric studies. The validity of the proposed method has been evaluated using the XFDTD software.

REFERENCES

1. Yee, K. S., "Numerical solution of initial boundary value problems involving Maxwell's equations in isotropic media," *IEEE Trans. Antennas and Propagation*, Vol. 14, 302–307, May 1966.
2. Taflove, A. and M. E. Brodwin, "Computation of the electromagnetic fields and induced temperatures within a model of the microwave-irradiated human eye," *IEEE Trans. Microwave Theory and Tech.*, Vol. 23, 888–896, Nov. 1975.
3. Taflove, A., "Application of the finite-difference time-domain method to sinusoidal steady-state electromagnetic penetration problems," *IEEE Trans. Electromagnetic Compatibility*, Vol. 22, 191–202, Aug. 1980.
4. Taflove, A. and S. C. Hagness, *Computational Electrodynamics: The Finite-difference Time-domain Method*, 3rd edition, Artech House, Norwood, MA, 2005.
5. Gandhi, O. P. and J. Y. Chen, "Electromagnetic absorption in the human head from experimental 6-GHz handheld transceivers," *IEEE Trans. Electromagnetic Compatibility*, Vol. 37, 547–558, Apr. 1995.
6. Jensen, A. and Y. Rahmat-Samii, "EM interaction of handset antennas and a human in personal communications," *Proc. IEEE*, Vol. 83, 7–17, Jan. 1995.
7. Dimbylow, P. J. and S. M. Mann, "SAR calculations in an anatomically realistic model of the head for mobile communication transceivers at 900 MHz and 1.8 GHz," *Phys. Med. Biol.*, Vol. 39, No. 9, 1537–1553, 1994.
8. Chuang, H. R., "Human operator coupling effects on radiation characteristics of a portable communications dipole antenna," *IEEE Trans. Antennas and Propagation*, Vol. 42, 556–560, Apr. 1994.
9. Nikita, K. S., G. S. Stamatakos, N. K. Uzunoglu, and

A. Karafotias, "Analysis of the interaction between a layered spherical human head model and a finite-length dipole," *IEEE Trans. Microwave Theory and Tech.*, Vol. 48, 2003-2013, Nov. 2000.

10. Rahmat-Samii, Y. and K. W. Kim, "Antenna and human in personal communications: Application of modern EM computational techniques," *Proc. IEEE*, 36–55, 1999.
11. Chen, W. T. and H. R. Chuang, "Numerical Computation of human interaction with arbitrary oriented superquadric loop antenna in personal communications," *IEEE Trans. Antennas and Propagation*, Vol. 46, 821–828, Jun. 1998.
12. Roa, S. M., D. R. Wilton, and A. W. Glisson, "Electromagnetic scattering by surfaces of arbitrary shapes," *IEEE Trans. Antennas and Propagation*, Vol. 30, 409–418, 1982.
13. Wong, K. L., *Planar Antennas for Wireless Communications*, Chapter 2, John Wiley & Sons, 2003.
14. Sadiku, M. N. O., *Numerical Techniques in Electromagnetics*, Chapter 5, CRC Press, 2001.
15. Makarov, S. N., *Antenna and EM Modeling with MATLAB*, Chapter 10, John Wiley & Sons, 2001.
16. Balanis, C. A., *Advanced Engineering Electromagnetics*, Chapter 2, John Wiley, New York, 1989.
17. Gabriel, S., R. W. Lau, and C. Gabriel, "The dielectric properties of biological tissues: II. Measurements in frequency range 10 Hz to 20 GHz," *Phys. Med. Biol.*, Vol. 41, 2251–2269, Dec. 1966.
18. Su, D. Y., D. M. Fu, and D. Yu, "Genetic algorithms and method of moments for the design of PIFAs," *Progress In Electromagnetics Research Letters*, Vol. 1, 9–18, 2008.
19. Jeon, S.-G., D.-H. Seo, Y.-S. Yu, and J.-H. Choi, "Broadband internal antenna for mobile DTV handsets," *PIERS Online*, Vol. 3, No. 7, 1048–1052, 2007.
20. Remcom Inco., XFDTD, http://www.remcom.com.